Wear xxx (xxxx) xxx–xxx

Contents lists available at ScienceDirect

Wear

journal homepage: www.elsevier.com/locate/wear

The effect of temperature on sliding wear of self-mated HIPed Stellite 6 in a simulated PWR water environment

V.L. Ratia[a,*], D. Zhang[a], M.J. Carrington[a], J.L. Daure[a], D.G. McCartney[a], P.H. Shipway[a], D.A. Stewart[b]

[a] University of Nottingham, Faculty of Engineering, University Park, Nottingham NG7 2RD, United Kingdom
[b] Rolls-Royce plc, Derby, United Kingdom

ARTICLE INFO

Keywords:
Sliding wear
Stellite 6
Cobalt based alloys
Electron backscatter diffraction

ABSTRACT

Cobalt-based Stellite alloys are widely used in the primary circuit of pressurised water reactors (PWR) to protect valve surfaces against wear and galling in a corrosive environment. In this study, self-mated sliding wear of HIP-consolidated (Hot Isostatically Pressed) Stellite 6 (Co - 27.1 Cr - 1.5 Si - 5.0 W - 0.96 C, in wt%) was investigated. A pin-on-disc apparatus was enclosed in an autoclave for wear testing, which was conducted in lithiated water from room temperature up to 250 °C (a representative PWR environment). Samples were characterized before and after wear testing using mass measurements, profilometry, X-ray diffraction and scanning electron microscopy (SEM) with electron backscatter diffraction (EBSD). The bulk HIPed alloy is predominantly two phase and comprises a cobalt-rich fcc matrix and an M_7C_3 carbide phase. However, surface grinding prior to wear testing causes a surface layer of the matrix to partially transform to a hcp cobalt-rich phase. The wear (mass loss) is very low below 150 °C but increases by approximately an order of magnitude when the temperature is increased from 150° to 250°C. SEM/EBSD reveals sub-surface damage and partial fcc to hcp transformation of the Co-rich matrix phase to a depth of ~ 15 μm in the disc. However, there is little change in transformation behaviour and depth with temperature and this is not regarded as a significant cause of the increased wear. The order of magnitude increase in wear is instead ascribed to a tribocorrosion mechanism associated with significantly higher corrosion rates at 250 °C than at 150 °C. As the material removal and factors affecting it are found to be significantly dependent on temperature, this work demonstrates the necessity of conducting assessments of materials for use in PWR environments under representative conditions.

1. Introduction

Due to their excellent combination of wear and corrosion resistance, cobalt alloys such as Stellite 6 (typical chemical composition of Co - 28 Cr - 4.5 W - 1.2 C - 0.5 Fe - 1.3 Si (in wt%) [1]), are employed as materials for the hardfacing of valves in the primary circuit in nuclear pressurised water reactors (PWRs) where reliability of the components is of critical importance. However, although they exhibit high resistance to wear, any debris removed from such components in a PWR primary circuit can result in a significant health and safety issue. As the wear debris travels round the primary circuit it passes through the core and the transmutation of cobalt-59 into its γ-emitting isotope cobalt-60 becomes a major source of radiation dose for plant maintenance workers [2]. The degradation behaviour, as a result of wear and corrosion, of various components in PWR environments has been examined in several studies [3–6] and over the past thirty years research has been undertaken on the development of low-cobalt hardfacing alloys to reduce the radiation exposure of maintenance personnel [7–11]. However, a fully acceptable replacement alloy for deployment in PWR plant remains elusive because Stellite 6 has an exceptional combination of resistance to both wear and corrosion that cannot be readily replicated. In such studies, Stellite 6 is often the reference material [7–11], but the information regarding Stellite 6 itself tends to focus on the rate of wear, with a somewhat more limited analysis of the mechanisms of wear. In contrast, there is significant literature addressing the mechanisms of wear of Stellite 6 under other conditions, such as dry sliding or sliding in water (or aqueous solutions) under atmospheric conditions. However, it is recognised that whilst the use of dry conditions in testing (such as sliding or galling tests) may be considered to simulate the worst-case scenario conditions for materials used in water-wetted bearings etc. (perhaps encountered when the lubrication has failed), the mechanisms of wear are highly dependent upon the environment and

* Corresponding author.
E-mail address: vilma.ratia@nottingham.ac.uk (V.L. Ratia).

https://doi.org/10.1016/j.wear.2018.09.012
Received 30 April 2018; Received in revised form 20 September 2018; Accepted 29 September 2018

temperature and so care must be taken in interpretation of results from such tests and their extrapolation to predict behaviour under the conditions of service experienced in a PWR. Accordingly, given the relative paucity of literature related to wear of Stellite 6 under such conditions, this introduction will seek to summarise relevant literature which addresses wear, corrosion and tribocorrosion of Stellites, with a focus on Stellite 6.

1.1. Wear of Stellite alloys

It has been argued that the reliability of cobalt alloys in sliding contacts stems from their exceptional galling resistance. In the case of Stellite 6, this has been attributed primarily to the behaviour of the cobalt-rich matrix rather than the hard phase volume fraction or the overall hardness. The metastable face centred cubic (fcc) structure of typical cobalt-rich matrices exhibits a high strain hardening ability and can transform to a hexagonally close packed (hcp) structure, restricting crack propagation [12]. Moreover, the hcp structure has fewer slip systems, aiding wear resistance in metal-to-metal contact. Smith et al. [13] studied the strain induced phase transformations in a cobalt alloy (Co - 30 Cr - 4 W - 1.1 C - 1.5 Mo - 3 Ni - 1.5 Si - 1 Mn (in wt%)) and an iron alloy (NOREM02) and their stability at temperatures up to 825 °C by in-situ X-ray diffraction and concluded that the transformation to hcp occurred at temperatures up to around 700 °C in the cobalt alloy, which is beneficial for applications at high temperatures.

The strain hardening ability and galling resistance increase as the stacking fault energy (SFE) decreases, since this limits dislocation cross-slip and climb. The SFE is controlled by the composition of the matrix; for example, Bhansali and Miller [14] demonstrated an increase in the SFE by adding nickel to Stellite 6 alloy which did not significantly affect its hardness but resulted in a decrease in galling resistance.

Persson [15] and Persson et al. [16,17] studied the mechanisms of tribological damage in Stellite 6 and Stellite 21 (Co - 27.6 Cr - 0.25 C - 5.3 Mo - 2.5 Ni - 0.92 Si - 0.8 Fe - 0.67 Mn (in wt%) [16]) and concluded that under dry sliding conditions, the alloys form a preferentially oriented, easily sheared superficial layer, where the basal planes of the hcp cobalt-rich matrix are parallel to the shearing direction. This layer is constantly regenerated and thus restricts the material transfer to a very thin layer, aiding in wear resistance. Beneath the superficial layer, there is a thick deformation hardened and phase transformed layer, which carries the applied load. Persson also reported the presence of an oxide layer [15], but concluded that the oriented shear layer had a more significant effect on the wear behaviour than the presence of the oxide layer.

It is generally accepted that the nature of oxide layer formation plays a role in the wear of cobalt alloys, especially at elevated temperatures. In their dry sliding wear studies on Stellite 1 (cobalt based material with nominal chemical composition in wt% 28.0–32.0 Cr, 11.0–13.0 W, 2.0–3.0 C, 3.0 Ni, 1.0 Si, 2.5 Fe and 1.0 Mn) at temperatures up to 700 °C, Conceiç ão and D'Oliveira [18] found that as the temperature was increased above 500 °C, rapid oxide formation resulted in the formation of a protective oxide debris layer which effected a reduction in both the coefficient of friction and the rate of wear. Similarly, Birol [19] attributed the superior elevated temperature sliding wear resistance of Stellite 6 (in comparison to both a nickel-based alloy and a hot work tool steel) to the nature of the oxide layer formed on the surface. In their elevated temperature metal-to-metal sliding wear tests in air, Crook and Li [20] observed that cobalt-chromium alloys exhibited a maximum rate of wear at 250 °C; they suggested that in these alloys, SFE increases with increasing temperature (resulting in higher rates of wear), but that formation of a protective oxide is also favoured by an increase in temperature, with the effect of the protective oxide dominating as the temperature was increased above 250 °C. Stott et al. [21] observed similar effects in the self-mated dry sliding of Stellite 31 and argued that above 250 °C, a stable thermally softened oxide glaze formed on the surface resulting in low rates of wear.

1.2. Corrosion of Stellite alloys

The corrosion behaviour of Stellite 6 in simulated PWR-water at high temperature up to 300 °C and pressure has been studied by several authors, with such water having a low oxygen-content and containing LiOH (used to to control the pH) or a combination of LiOH and H_3BO_3 (used as a neutron absorber). Oxide film growth in reducing conditions is believed to occur predominantly by solid state diffusion, and preferential dissolution of cobalt [22–25]. The observed oxide layer has been found to be rich in chromium and depleted in cobalt, pointing to a preferential dissolution of cobalt at the oxide-solution interface [23,25,26]. Moreover, much thicker oxide layers are observed on the matrix in comparison to the carbides after long exposures [26]. X-ray photoelectron spectroscopy has revealed that Cr_2O_3 and CoO are commonly found close to the top surfaces of the oxide layers [24–26], with both short and long exposure times leading to oxide layers with similar compositions [24].

The corrosion rates and mechanisms are also very sensitive to temperature. Taylor and Armson [25] observed that cobalt release rates in the Stellite alloys examined were smaller by a factor of approximately 10 at 180 °C in comparison to 250 °C after exposure for a week whereas, there was only a relatively small difference in the cobalt release rates at 250 °C and 290 °C. However, the underlying mechanisms were not discussed.

1.3. Tribocorrosion of Stellite alloys

Where they occur together, corrosion and mechanical wear cannot be considered independently, as they may exhibit synergetic effects (known as tribocorrosion). It has been proposed [27,28] that tribocorrosion of Stellite alloys in PWR conditions is associated with both material loss and growth of oxide layers by corrosion and the subsequent mechanical removal of these passivating oxide films by wear. Xu et al. [29] conducted electrochemical measurements of the corrosion rate of UNS R30006 (analogue of Stellite 6) in simulated PWR conditions following application of a very mild wear event (involving rotations of cylinder end faces in contact under a very small nominal pressure of 1.4 kPa) which was used to disrupt / remove any protective oxide layers from the contact. Whilst the corrosion behaviour was seen to be dependent upon the precise water chemistry of the system, a general observation was that there was no significant increase in corrosion rates at low temperatures (25 °C and 65 °C), but that at 150 °C, 200 °C and 250 °C, significant increases in corrosion rate were observed (up to around eight times of that observed before the wear event), with the rates decaying to the values observed before wear after approximately 20 min.

Lemaire and Calvar [30] studied the behaviour of Stellite 6 in the field in control rod drive mechanisms in a PWR and also in a laboratory loop study, and suggested that tribocorrosion effects explained the differences in behaviour in the two situations, with wear increasing with the number of depassivation events and time for material dissolution before repassivation. Guadalupe Maldonado et al. [31] studied the tribocorrosion of Stellite 21 type CoCrMo alloy in a H_2SO_4 solution at room temperature under a range of conditions and reported that wear increases when a passive film forms on the surface, irrespective of the potential having been applied or not. The film was found to increase the mechanical wear by about an order of magnitude, and this was attributed to wear-accelerated corrosion, but also to a significant increase in subsurface deformation of the metal when a passive film was present.

1.4. Aims of this work

The mechanisms of wear occurring in Stellite 6 in a high-temperature high-pressure water environment are still not well understood. Accordingly, the aim of this study is to characterize the wear rates and

Table 1
Chemical composition of HIPed Stellite 6 determined by inductively coupled plasma (ICP). Carbon was determined by combustion infrared detection (carbon).

Element	Co	Cr	Fe	Ni	Si	W	C
wt [%]	bal.	27.08	0.73	0.87	1.47	5.01	0.96

*also included Cu and Mn are < 0.1 wt%.

mechanisms of wear of self-mated Stellite 6 as a function of temperature (between room temperature and 250 °C) in simplified simulated PWR conditions, namely deoxygenated and lithiated water.

2. Experimental procedure

2.1. Materials

The material examined in this work was a cobalt alloy denoted as Stellite 6. A commercially available powder was manufactured into solid by hot isostatic pressing (HIPing) and supplied by LSN Diffusion (Llandybie, UK). Compositional analysis of the HIPed material was conducted by AMG Analytical Services (Rotherham, UK), the results of which are presented in Table 1.

2.2. Experimental methods

2.2.1. Wear testing

Wear testing was conducted in an autoclave pin-on-disc wear tester which allowed testing to be conducted at elevated temperatures in an aqueous environment. Both the pin and the disc were manufactured from the same material stock. In the test setup, shown in Fig. 1, a disc of 30 mm diameter (with a ground surface, Ra ~ 0.4 μm) is mounted in a rotating sample holder, and a 10 mm diameter pin (which has a 50 mm radius spherical cap ground onto one of the end faces) is loaded against the rotating disc via a 4 kg stainless steel dead load contained within the autoclave. A load stabilising mechanism allowing freedom of vertical movement ensures that the loading remains constant throughout the test. Buoyancy effects on the dead loading result in small changes in contact load with temperature as a result in changes in the densities of both the water and the steel; the contact force varies between 34.8 and 37.1 N.

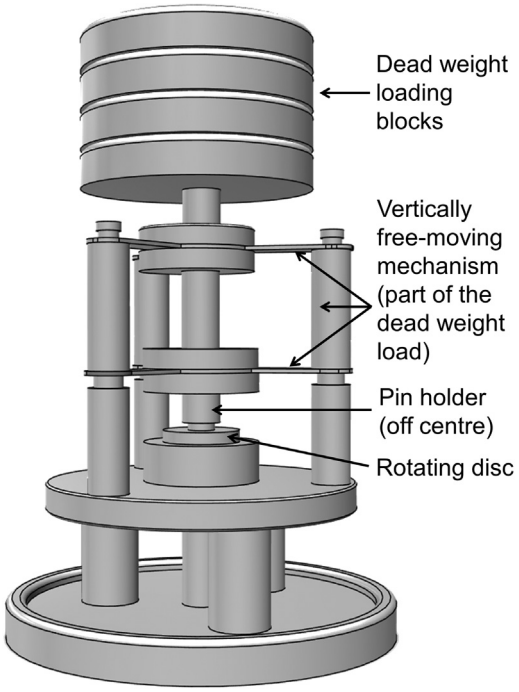

Fig. 1. Schematic diagram of the pin-on-disc apparatus which was enclosed in an autoclave for wear testing.

The wear test system is immersed in deoxygenated deionised water with an addition of 8.5 mg of LiOH per litre resulting in the solution having a pH of approximately 10.5 at room temperature when prepared. There was no addition of boric acid. A range of water temperatures (measured via a thermowell inside the autoclave) were employed as follows: room temperature (~ 20 °C), 80 °C, 150 °C, 200 °C and 250 °C. The pressure in the system was built up autogenously (i.e. no external pressurisation was employed). The rotation of the disc is driven through a magnetic coupling with an external drive with a constant value of 200 rpm being employed. The offset of the axis of loading and the axis of rotation is 10 mm, resulting in a wear track diameter of 20 mm and a sliding speed of 0.21 m s^{-1}. Two testing durations (either 5 or 24 h) were employed, corresponding to approximate sliding distances of 3770 and 18100 m, respectively. Normally, two test repetitions were carried out under each set of testing conditions. The wear was measured by mass loss measurements of both the pin and the disc with a balance with 0.1 mg precision. In addition to the mass loss measurements, profilometry was conducted on the disc samples to verify the trends in mass losses.

To assess the mass change from corrosion only, an exposure test of a disc sample in deoxygenated lithiated water without sliding contact was conducted at 250 °C for 24 h. The disc was mounted into the disc holder and was rotated as it would be in a wear test, but without any pin contact. Heating of the system took approximately 5.5 h, the sample was held at 250 °C for 24 h, and the system was allowed to cool down, which took up to 17 h.

2.2.2. Materials characterisation

Macrohardness of the bulk material was measured with a Vickers hardness tester with 20 kgf load. The value presented is an average of not less than ten measurements.

Microstructures and the worn surfaces of both the pin and the disc were examined with a JEOL 6490LV scanning electron microscope (SEM), using both secondary electron (SE) and backscattered electron (BSE) imaging. Energy dispersive X-ray analysis (EDX) was used to identify the composition of features of interest. More detailed analysis of the worn surfaces was also conducted with a JEOL 7100F field emission gun SEM (FEG-SEM). To obtain information regarding changes in phase proportions and grain orientations in the materials following wear, electron backscatter diffraction (EBSD) was utilised with an accelerating voltage of 15 kV and a step size of 0.06 μm for wear scars (Fig. 9) and 0.10 μm for bulk material (Fig. 2), along with Aztec acquisition software.

X-ray diffraction (XRD) was used to determine the phase make-up of the alloys and of the wear tracks. For large area analysis, a Bruker D500 diffractometer with monochromatic Cu-Kα radiation was used with a 40 kV tube voltage and a 25 mA tube current, a step size of 0.01° and a step dwell time of 7 s. For point source XRD (where diffraction information is gathered from an area with a maximum length of up to ~2.5 mm), a Bruker-AXS D8 Discover with Cr-Kα radiation was used with a 30 kV tube voltage and a 35 mA tube current, a step size of 0.04° and a step dwell time of 15 s.

Profilometry was conducted on the discs following wear to allow the volume loss of the discs to be estimated, which permitted direct comparison with the gravimetric changes recorded. A Taylor Hobson Form 50 Talysurf stylus profilometer was used to obtain typically four profiles across the wear scars of a representative worn sample tested at each condition (temperature and test duration combination) with the wear volume able to be estimated from the average cross-sectional area of the track and the track circumference.

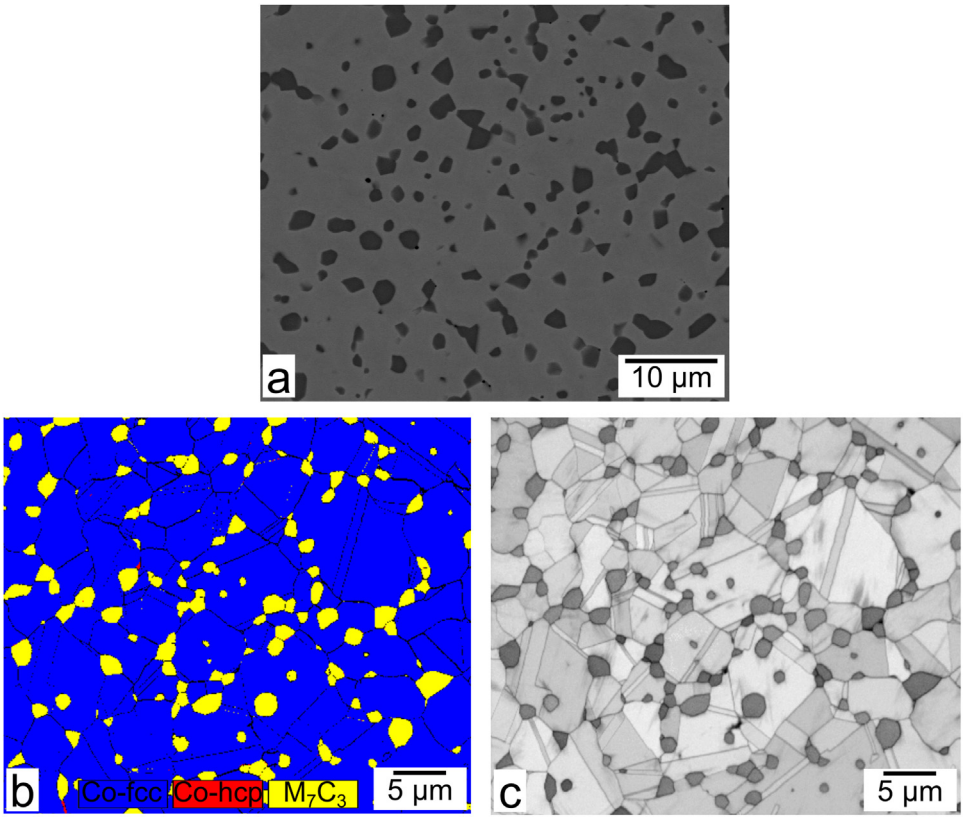

Fig. 2. Microstructure of Stellite 6; (a) BSE image; (b) EBSD derived phase composition map with fcc matrix (indicated by the dark grey areas; coloured blue online) and M_7C_3 type carbides (indicated by the light grey areas; coloured yellow online); (c) EBSD derived band contrast image showing the carbide phase, matrix grain structure and twinning present in the matrix.

3. Results

3.1. Materials characterisation

Fig. 2a is an SEM BSE image of Stellite 6, showing that the microstructure consists of chromium-rich carbides (dark contrast areas in the image due to their lower mean atomic number) in a cobalt-rich matrix. The macrohardness of the pins and the discs were 400 ± 2 and 401 ± 2 HV20, respectively.

The carbides are seen to be generally equiaxed and approximately 1–5 μm in size. The volume fraction of carbides was measured from the BSE images using ImageJ Fiji software [32] and was found to be 13 ± 2 vol%, slightly less than the value of 17.9 ± 1.7% reported by Ahmed et al. [33]. SEM-EDX analysis showed that the carbides are chromium-rich; according to Ashworth et al. [34], the metal in the carbides in HIPed Stellite 6 type alloy consists of 80–85 at% chromium with the remainder being cobalt, tungsten, and iron.

An EBSD phase map of the microstructure is presented in Fig. 2b, which shows that in the as-polished condition, the cobalt-rich matrix is predominantly fcc (indicated by dark grey areas; coloured blue online) and the carbides are of M_7C_3 type (indicated by the light grey areas; coloured yellow online). The band contrast (BC) image of the same area (shown in Fig. 2c) reveals that the matrix also exhibits twinning.

Fig. 3 shows the XRD patterns of both a polished and a ground surface of Stellite 6. These show that the dominant peaks belong to the metallic matrix, with the M_7C_3 type carbide peaks being relatively low in intensity. The polished and ground surfaces are distinctly different in terms of the phases present in the metallic matrix. In the polished state, only fcc peaks are clearly visible (in accord with the EBSD phase map presented in Fig. 2b), whereas the ground surface indicates that the matrix exhibits both fcc and hcp structures. Moreover, grinding of the surface results in broadening of the XRD diffraction peaks in comparison to those from a polished surface, indicative of nanometre grain size and/ or microstrain in the material.

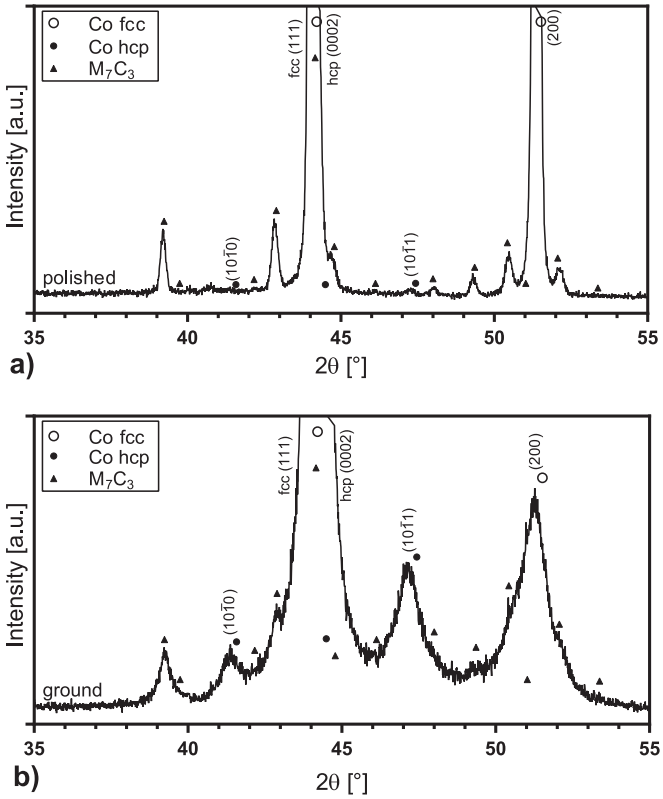

Fig. 3. XRD patterns of Stellite 6 (normalised to M_7C_3 peak at 39.2°) with Cu-Kα radiation, with Miller (fcc) or Miller-Bravais (hcp) indices presented for the cobalt phase peaks; (a) polished surface; (b) ground surface.

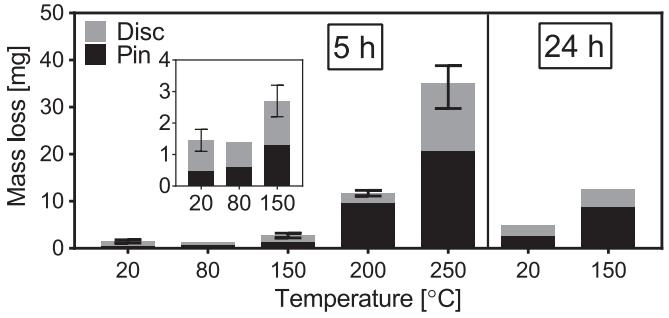

Fig. 4. Average mass losses of Stellite 6 wear test samples tested at a range of temperatures for both 5 and 24 h (the insert shows detail relating to the mass losses at low temperatures). The error bars represent minimum and maximum values of the total wear.

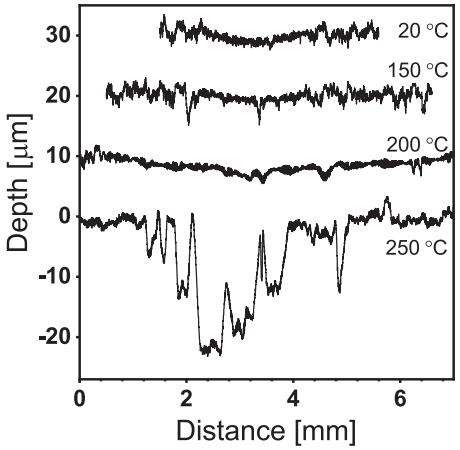

Fig. 5. Disc wear scar profiles of samples tested at 20, 150, 200 and 250 °C for 5 h.

3.2. Wear behaviour

3.2.1. Mass loss results

Fig. 4 presents mass loss measurements of the samples after autoclave wear tests as a function of temperature, and shows that the wear rate increases significantly once the temperature exceeds 150 °C. The total wear of the pin and the disc at 250 °C is more than ten times that observed at 150 °C. The mass loss from the pin and the disc are often significantly different. It is notable that there was a significant increase (~ seven times) in the average mass loss of the pin as the temperature was raised from 150 °C to 200 °C, but that the mass loss of the disc was similar at these two temperatures. However, a similar increase (~ seven times) in the average mass loss of the disc itself was seen as the temperature was raised from 200 °C to 250 °C.

Where the mass losses in the 5 h tests were small (i.e. at low temperatures), the original grinding marks were still visible on the surface following the wear test, and thus a meaningful analysis of the wear was not achievable. As such, additional wear tests were conducted for an extended time of 24 h at both 20 °C and 150 °C, with the resulting wear being sufficiently deep to remove the effects of the grinding marks. Especially at 20 °C, the average total wear rate was less for the 24 h tests than it was for the 5 h tests indicating that the wear of the surface-ground material was more rapid than that of the bulk material.

It was recognised that, as well as the effects of tribocorrosion, general corrosion of the sample surfaces (outside the wear track) may also affect the mass loss measurements. To assess the significance of this, mass loss measurements on samples exposed to lithiated high temperature water without sliding contact were conducted. For the disc sample exposed at 250 °C for 24 h, the mass loss of the disc was 0.2 mg, from which it can be estimated (based upon a ratio of surface areas) that the mass loss of the disc and pin pair in a 24 h test solely due to corrosion will be less than 0.3 mg.

The minimum overall mass loss following a wear test in the water-wetted environment (observed at room temperature) was 1.5 mg. Therefore, it can be seen that both the experimental measurements, and the estimates based upon work reported in the literature, indicate that the mass loss associated with corrosion itself can be deemed negligible compared to that resulting from wear and/or tribocorrosion.

3.2.2. Profilometry of the wear scars

Fig. 5 presents representative cross sectional profiles of the wear scars on the discs tested for 5 h at 20, 150, 200 and 250 °C; in accord with Fig. 4, these show a relatively small amount of wear at the lower temperatures, along with a clear increase in the size of the disc wear scar between 200 °C and 250 °C; to give an indication of the scale of the change in behaviour with temperature, it is noted that the average maximum depths were 2.6 μm, 5.7 μm, 5.3 μm and 21.9 μm for the four temperatures examined (20, 150, 200 and 250 °C respectively). The worn depths can be compared with the scale of subsurface damage as presented in Fig. 9.

3.3. Characterisation of wear scars

The surfaces of wear scars were examined, with those from the tests at the highest and lowest temperatures being examined in detail. For the tests at 20 °C, the surface was examined following wear for 24 h (due the low amounts of wear after the 5 h tests). However, for the tests conducted at 250 °C, the scars following testing for 5 h were examined. Both the disc and pin surfaces were examined after the wear tests. Also, debris remaining on the surface of the disc when the test was stopped was collected and analysed.

3.3.1. Wear surfaces

SEM investigations of the wear tracks showed that there was no clear evidence of the formation of a distinct wear debris layer on the worn surfaces of the samples at any of the testing temperatures; the microstructure of a matrix with carbides was visible across the wear scars in all cases. Examples of this can be seen in Fig. 6a–d, where plan view wear surface images obtained from pin samples tested at the lowest (20 °C) and the highest (250 °C) testing temperatures are presented. At all temperatures, the majority of the wear scar areas were relatively flat, with some deeper scratches present; when viewed at the macroscale, the sample tested at 250 °C had deeper and more frequent scratches. Given the very different rates of wear at these two temperatures, the worn surfaces are surprisingly similar in appearance, and as such, there is little evidence to support a change in the fundamental mechanism of material removal as the temperature is changed. At all temperatures, the wear scars indicate that the carbides and matrix exhibit recession at very similar rates (i.e., there is no preferential recession of one phase against the other).

When observed using SEM, all wear scars (irrespective of the test temperature) contained several different distinct features. These features could generally be separated into four categories: oxidised areas (seen as dark formations on the wear surface), carbide pull out, scratching, and smoother regions. The wear scars on the pins and the discs were generally very similar in appearance; Fig. 7 shows plan view SEM images of the wear scars on a pin and a disc tested at 250 °C for 5 h. It can be seen that a large part of the wear surface is rather smooth in both of the samples and that both the pins and the discs undergo carbide pullout (Fig. 7c–d), which may trap debris within the voids left on the surface, as in Fig. 7c.

3.3.2. Microstructural characterisation after wear tests

Point source XRD was conducted on the Stellite 6 discs both inside and outside the wear track to determine the nature of any phase

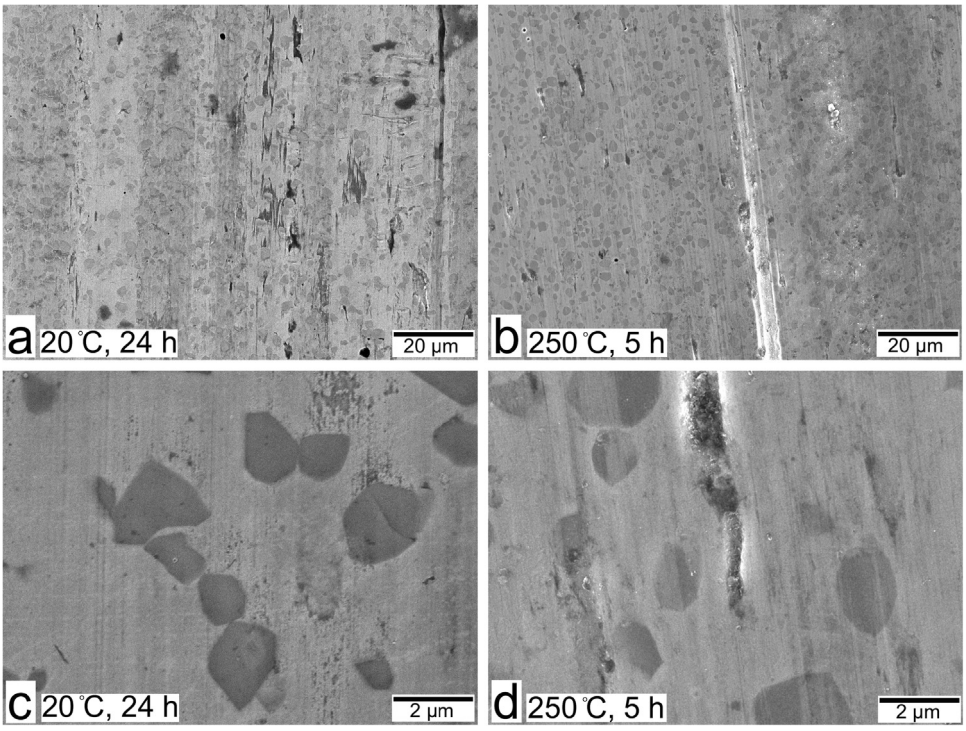

Fig. 6. Plan view SEM micrographs (SE) of the wear scars on pin samples at low and high magnification; (a, c) scars following wear at 20 °C for 24 h; (b, d) scars following wear at 250 °C for 5 h.

transformations which had taken place during wear and the diffractograms are presented in Fig. 8. When comparing with Fig. 3, it should be noted that the 2θ range employed of 70–85° with Cr-Kα radiation corresponds to a 2θ range of 45.4–54.1° with Cu-Kα radiation. Thus, the hcp peak with $(10\bar{1}1)$ indexing at 73.4° (Cr-Kα) corresponds to the peak at 47.4° (Cu-Kα), and the fcc peak with (200) indexing at 80.5° (Cr-Kα) corresponds to the peak at 51.5° (Cu-Kα). This 2θ range was selected as the two cobalt peaks do not overlap with each other and are representative of the fcc and hcp structures in this material. A reduction in the fcc peak intensity and the corresponding increase in the hcp peak intensity indicates that the wear process causes a phase transformation to hcp in the matrix at both temperatures and it is notable that for wear at 20 °C, the transformation to hcp increases with test duration.

In light of the XRD evidence, electron backscatter diffraction (EBSD)

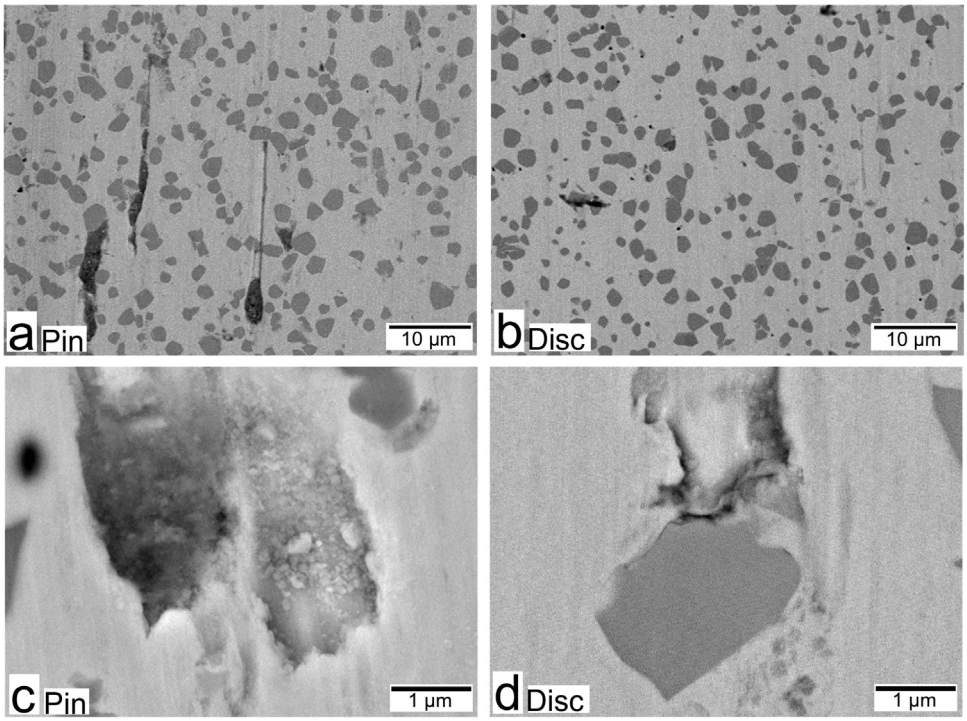

Fig. 7. Low and high magnification plan view SEM micrographs (BSE) of the scars following wear at 250 °C for 5 h; (a, c) scars on pin sample; (b, d) scars on disc sample.

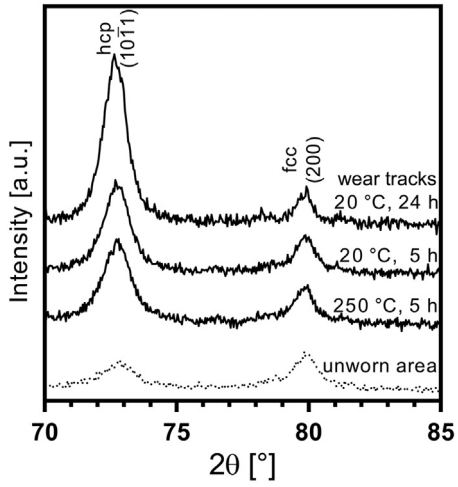

Fig. 8. XRD patterns obtained with a point source Cr-Kα radiation within the wear track of the samples tested for 5 h at 20 °C and 250 °C, and for 24 h at 20 °C. Alongside is an XRD pattern from an unworn area of a sample tested for 5 h at 20 °C (dotted line). The Miller (fcc) and Miller-Bravais (hcp) indices are indicated for the peaks associated with the cobalt-rich matrix.

was used to investigate the extent of the fcc to hcp phase transformation below the worn surface. In Fig. 9, sub-surface sections are shown for an unworn region (a), and for wear tracks following testing at both 20 °C and 250 °C ((b) and (c) respectively). In all cases, forward-scatter detector (FSD) images and EBSD derived band contrast (BC) and phase maps are presented. Band contrast images indicate grain boundaries and regions of crystallographic damage (e.g., regions of heavy deformation with high dislocation densities); twinning of matrix grains is evident from the fine parallel lines in the matrix phase. The phase maps indicate regions with different crystal structures, and here, three structures have been indexed, namely the fcc (dark grey regions; coloured blue online) and hcp (medium grey regions; coloured red online) forms of the cobalt-rich matrix and the M_7C_3 carbides (light grey regions; coloured yellow online). Regions that cannot be indexed (generally associated with high levels of crystallographic damage) are shown by black pixels.

The phase maps show that (in accordance with the XRD evidence presented in Fig. 3) the initial ground surface exhibits surface damage with some hcp matrix close to the surface, which has transformed from the bulk fcc matrix material (Fig. 9a). The BC and phase maps (Fig. 9b) show that following wear for 24 h at 20 °C, there is significant microstructural refinement and a greater degree of transformation from fcc to hcp in the matrix close to the worn surface, with this transformation being seen as far as 15 μm below the surface (far greater than the ~ 4.6 μm depth of wear at this temperature and duration). Following wear for 5 h at 250 °C, the sub-surface region exhibits even greater damage in the BC image; some of this region cannot be indexed in the phase map, suggesting that the matrix here is disordered with a high dislocation density due to plastic deformation (Fig. 9c). In addition to the unindexed regions, there is also indication of the fcc to hcp transformation having taken place, seen as red areas. The overall depth to which the phase transformation has occurred is quite similar at the temperatures of 20 °C and 250 °C, but near to the worn surface, hcp formation is more evident at the lower temperature (in accord with the XRD evidence presented in Fig. 8), noting the longer test duration.

3.3.3. Wear debris collected in the test

Fig. 10 shows BSE images of the wear debris collected from the wear tests at both 20 °C and 250 °C, along with EDX maps of the same regions. It is seen that following wear at 20 °C, the debris is very fine; the EDX analysis indicates that there is a significant oxygen level in the debris, indicating that it is an oxide of chromium and cobalt. Following wear at 250 °C, the wear debris was much coarser than that observed following wear at 20 °C; the EDX maps indicate a high oxygen level in the debris, again suggesting that it is an oxide of chromium and cobalt.

4. Discussion

The wear of self-mated Stellite 6 in lithiated water has been shown to be sensitive to the temperature of the water, with a significant increase in the rate of wear above a temperature of 150 °C (Fig. 4). As such, an assessment of the significance of various factors expected to play a role in determining the temperature dependence of wear in Stellite 6 will be made in the following section.

4.1. The role of material hardness

The wear behaviour of a couple typically exhibits a dependence upon the hardness of the materials [35], and as such, thermal softening needs to be considered as a potential cause of the increasing wear rate with temperature. Stellite 6 exhibits an approximately linear reduction in macrohardness of between 15% and 20% as the temperature is increased from room temperature to 250 °C [36,37]. In work examining other Stellite alloys, Kapoor et al. [38] and Liu et al. [39] sought to measure the temperature dependence of hardness of the cobalt-rich matrix phase and the carbide phase separately, and found that whilst areas with predominantly both phases exhibit a reduction in hardness with temperature, this is much more significant for the matrix phase (both in absolute terms, and as a proportion) with matrix hardness reductions of up to approximately 30 HV being seen on raising the temperature from room temperature to 250 °C.

The majority of the work reported in the literature which examines the effect of temperature on the sliding / galling wear behaviour of Stellites has been conducted in air, and thus the role of the hardness of the material is difficult to separate from the role of oxidation in any changes in behaviour observed. In the current work, the formation of thick oxide debris beds covering the wearing surfaces has not occurred due to the low oxygen content in the autoclave. The wear rate increases very significantly once the temperature is increased above 150 °C, but a similar discontinuity in hardness has not been reported in the literature; moreover, it is notable that the depth and degree of subsurface damage below the worn surface is not significantly different at 20 °C than it is at 250 °C (Fig. 9). It is therefore proposed that these observations indicate that the change in hardness is not a controlling factor in the change of wear rate with temperature as the temperature increases above 150 °C.

4.2. The role of phase transformation

The phase transformation from fcc to hcp (and in particular, the ability for this transformation to occur even at elevated temperatures [13]) is commonly considered to be one of the reasons for the excellent wear behaviour of cobalt alloys. However, in assessing the degree of phase transformation following wear of Stellite 6, care needs to be exercised in interpreting the XRD patterns, as the amount of fcc and hcp matrix in the prepared surface region is itself affected by the sample preparation processes and may not be representative of the bulk material; indeed, previous work [34] as well as results presented here (Fig. 3) show that surface grinding results in an increase in the hcp fraction whereas surface polishing results in a decrease in the hcp fraction.

Despite the initial ground surface of the wear test samples having a fraction of the matrix with an hcp structure (Fig. 8 and 9), a significant increase in the hcp fraction (and the depth to which the transformation to hcp has occurred) has been seen following wear (both at 20 °C and at 250 °C) via both XRD (Fig. 8) and EBSD phase mapping (Fig. 9), indicating that the wear process promotes the transformation.

Due to the sphere on flat arrangement employed, the contact conditions experienced at the end of the wear tests are dependent upon the

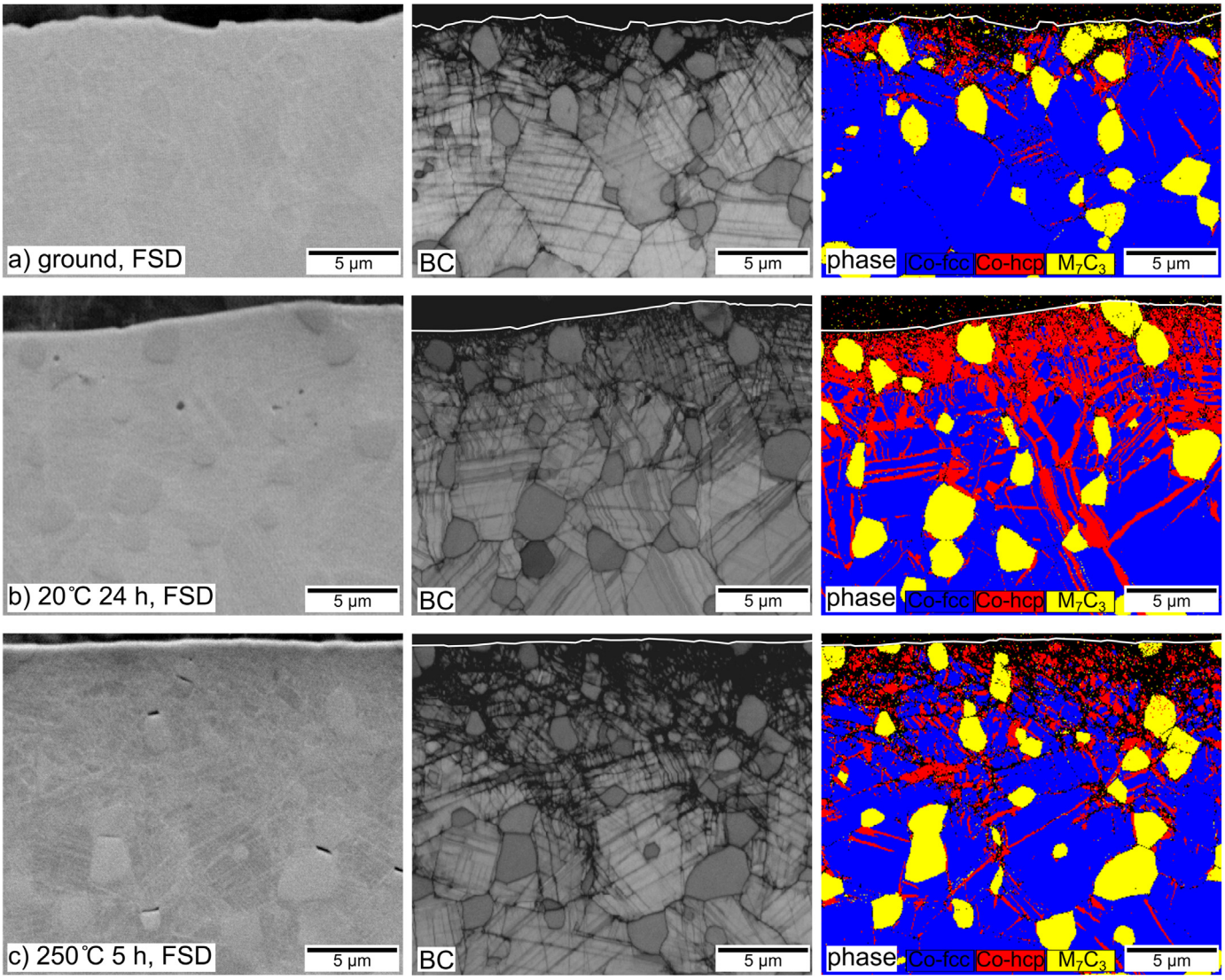

Fig. 9. Forward-scattered detector (FSD) image, EBSD derived band contrast and phase maps of cross sections of (a) a ground surface without wear, (b) a wear scar on a disc tested at 20 °C for 24 h and (c) wear scar on a disc tested at 250 °C for 5 h. The white line marks the surface of the sample. The direction of sliding is normal to the image plane. In the phase map, fcc matrix is coloured dark grey (blue online), hcp matrix is coloured medium grey (red online) and M_7C_3-type carbide is coloured light grey (yellow online).

amount of wear that has occurred up to that point since the contact area increases with wear. For example, at the end of a 24 h test at 20 °C, the contact pressure is approximately three times that at the end of a 5 h test at 250 °C. However, it can be seen that, despite the falling contact pressure due to wear, the degree of transformation to hcp following wear at 20 °C increased with increasing test duration (Fig. 8) and this indicates that the transformation is related to damage accumulation. However, Fig. 9 illustrates that the depth to which transformation to hcp has occurred is very similar at both 20 °C and 250 °C, although the degree of transformation to hcp close to the surface is higher at the lower temperature. Whilst there are differences in the wear-induced transformation behaviour as a function of temperature, the nature of the changes indicate that the phase transformation behaviour is not a dominant factor in the change of wear rate with temperature as the temperature increases above 150 °C.

4.3. The role of tribocorrosion

In lithiated water at elevated temperatures, corrosion films of Cr_2O_3 and CoO have been shown to develop on Stellite 6 [24]. Given the changes in the rate of wear, the appearance of the wear tracks following wear at 20 °C and 250 °C are very similar (Fig. 6), with a relatively smooth surface in both cases, and a not dissimilar level of sub-surface deformation (as seen in the BC images in Fig. 9). The appearance of the wear scars is also similar for the both pins and the discs in each case (Fig. 7), despite the fact that the contact conditions for the pin and disc are very different (the pin is in permanent contact with the disc, whereas a point on the disc is only in contact with the pin once every revolution – approximately every 0.3 s). As such, the tribocorrosion effects would be expected to be different for the disc than for the pin, since the disc has a large fraction of its time where the development of a chemical surface film will take place, which can then be removed by the intermittent contact with the pin; in contrast, the pin surface is in permanent contact with the disc which may result in less ready access of the chemical medium to the wearing surface. Given that the worn surfaces of the pin and disc are so similar, it is proposed that the wear process very effectively removes any films developed on the surfaces by corrosion; indeed, the wear debris observed after test at 20 °C (Fig. 10) is made up of very fine particles (sub-micron in size) and agglomerates of such particles which are rich in cobalt, chromium and oxygen (indicating that they originate from corrosion films formed on the surfaces); the debris particles from the 250 °C test are generally larger than

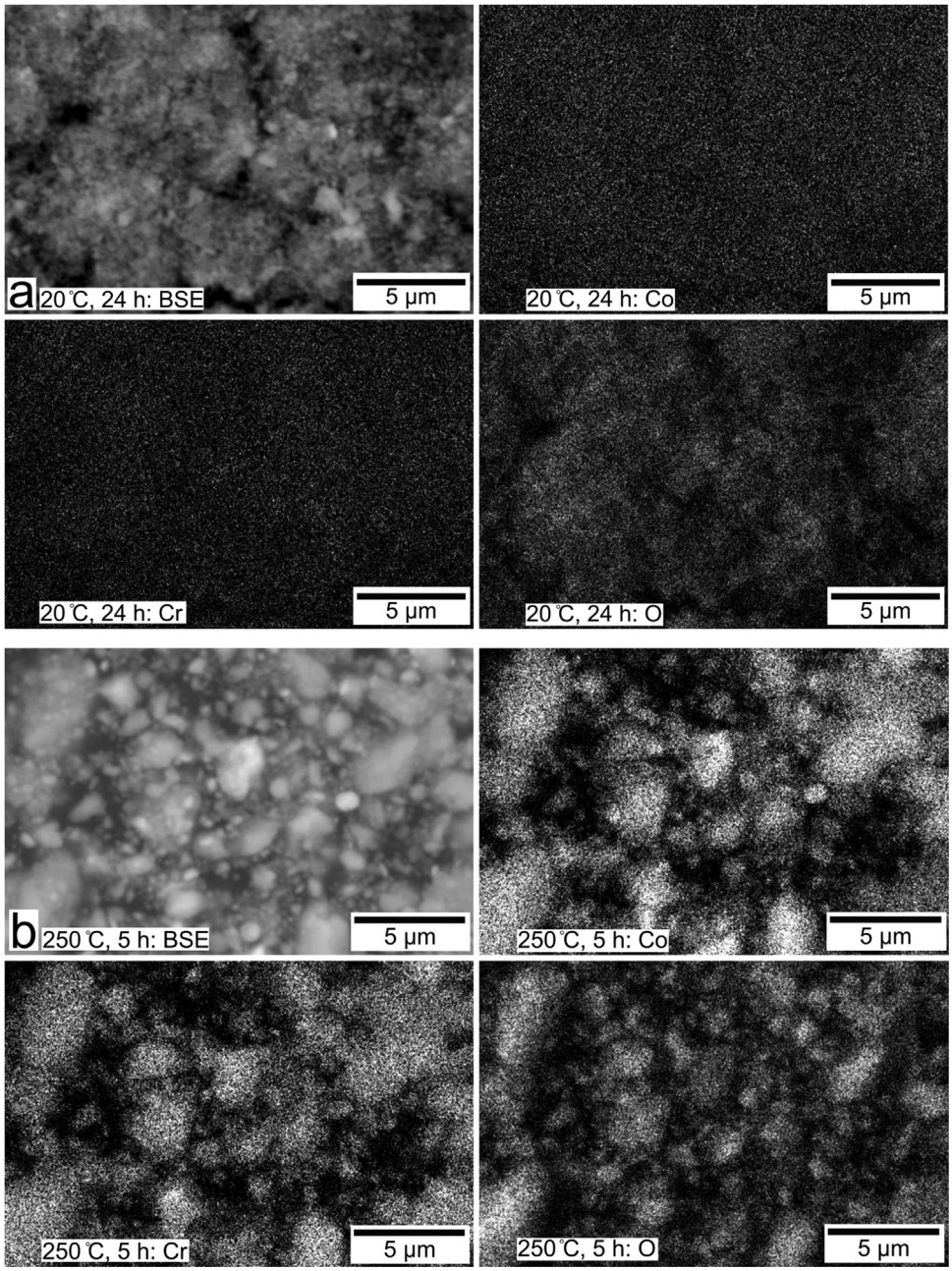

Fig. 10. BSE images and EDX maps for cobalt, chromium and oxygen of the wear debris: (a) following wear at 20 °C for 24 h and (b) following wear at 250 °C for 5 h.

those from the 20 °C test, indicating that corrosion has been more significant at the elevated temperature.

In seeking to understand the rapid increase in wear of Stellite 6 as the temperature increases above 150 °C, it is notable that the corrosion rate itself has been reported to exhibit similar rapid increases at temperatures close to 250 °C. From their week-long loop exposure tests of a variety of Stellites, Taylor and Armson [25] observed that there was a ten-fold increase in cobalt release rates between 180 and 250 °C, but a much less significant increase as the temperature was further increased to 290 °C.

In the current tests, corrosion affected the observed mass losses only to a negligible extent considering the accuracy of the scale, its effect being less than 0.3 mg for a pin-disc pair exposed for 24 h at 250 °C. To support this, the measured mass loss was compared with estimates from corrosion rates of Stellite 6 in simulated PWR conditions reported in the literature. The corrosion rate for a Stellite 6 weld deposit in simulated PWR water conditions at 360 °C for 1500 h was reported to be < 0.1 mg m^{-2} h^{-1} [40], leading to an estimate of a mass loss for the disc used in this work of less than 0.01 mg in a 24 h time period, although it is noted that the average corrosion rate is much larger as the test time is reduced [25]. Shorter exposure times were used by Maffiotte et al. [23], who reported the corrosion to be about 0.7 mg dm^{-2} in a 250 h test, corresponding to a mass loss of about 0.02 mg in 24 h for the disc used in this work. Finally, Xu et al. [29] estimated the initial corrosion rate of R30006 (a Stellite 6 analogue) at 250 °C to be about 11 µm $year^{-1}$ corresponding to a mass loss of about 0.6 mg in 24 h for the disc used in this work.

Iordache et al. [28] conducted sliding wear tests of Stellite 6 in a corrosive environment at 85 °C with different times between points on the surface coming into contact (what they termed the *latency period*) and found that higher latency periods resulted in an increase in wear rate. They proposed that wear occurred mainly by the mechanical removal of the thin Cr_2O_3 layer formed by corrosion, and that the mechanical wear of the metal beneath the oxide layer was itself

insignificant. By increasing the latency period by 1000 times, the total wear was observed to increase approximately 10-fold. Similarly, Lemaire and Calvar [30] reported that longer latency periods lead to an increase in the tribocorrosion rate of Stellite 6 under PWR-simulating conditions at between 200 °C and 250 °C. As the rate of corrosion increases with increasing temperature (resulting in thicker corrosion films [41]), it is proposed that the material removal rate will continue to increase until the film forms fast enough to withstand removal by wear, and thus becomes protective. Direct evidence of tribocorrosion was presented by Xu et al. [29] who studied the corrosion rates of UNS R30006 (the composition of which is very close to that of Stellite 6). They concentrated on the corrosion rate changes during and after wear, but did not report on the amount of wear itself. They found that at temperatures between 150 and 250 °C, the corrosion rates increased significantly during wear and remained high for a period after the wear event, but returned to the level observed prior to the wear event taking place after approximately 20 min; moreover, the significance of the increase in corrosion rate following a wear event was much lower at lower temperatures.

As such, it is suggested that the results observed in this work along with related evidence from the literature indicate that tribocorrosion is the dominant factor regarding the effect of temperature on the rate of wear of Stellite 6 under PWR-simulating conditions.

5. Conclusions

The wear rate of self-mated Stellite 6 sliding in lithiated water has been examined as a function of temperature. A significant increase in the rate of wear has been observed once the temperature exceeds approximately 150 °C. Whilst wear results in both sub-surface damage and transformation of the fcc matrix phase to an hcp structure to a depth of approximately 15 μm below the wearing surface, the differences in these with temperature are not considered to be primary factors in controlling the temperature dependence of the rate of wear. Instead, it is proposed that the significant increase in wear rate as the temperature is increased is due to higher corrosion rates at elevated temperature, and the removal of the corrosion product from the Stellite 6 surface by the action of wear, leading to a high rate of wear being observed. Given that the mechanisms and rates of material removal are so sensitive to temperature, this work highlights the importance of using representative conditions when conducting assessments of materials for use in PWR environments.

Acknowledgements

The authors are grateful for the financial support from Rolls-Royce plc. This work was supported by the Engineering and Physical Sciences Research Council [grant number EP/K005138/1], United Kingdom; and the University of Nottingham. The authors thank the Nanoscale and Microscale Research Centre (nmRC) for providing access to instrumentation. Dr. Nigel Neate and Dr. Hannah Constantin are gratefully acknowledged for setting up the point source XRD measurements.

References

[1] Deloro Wear Solutions GmbH, Technical data Stellite™ 6 alloy 2 p. 〈https://www.deloro.com/stellite-data-sheets/?Rq=stellite6〉.
[2] E. Baumann, I.R. Terry, The EPR: a clear step forward in dose reduction and radiation protection, Nucl. Eng. Des. 236 (2006) 1720–1727, https://doi.org/10.1016/j.nucengdes.2006.04.011.
[3] W.H. Roberts, Paper 20: measurement of sliding friction and wear in high-temperature high-pressure water environments, Proc. Inst. Mech. Eng. Conf. Proc. 180 (1965) 37–48, https://doi.org/10.1243/PIME_CONF_1965_180_318_02.
[4] D.J. DePaul, Corrosion and Wear Handbook for Water-cooled Reactors, McGraw-Hill, New York, 1957.
[5] H.H. Heath, Bearings for nuclear engineering, Proc. Inst. Mech. Eng. Conf. Proc. 182 (1967) 449–459, https://doi.org/10.1243/PIME_CONF_1967_182_034_02.
[6] S. Hother-Lushington, D.W. Garside, P. Sellors, Paper 12: water-lubricated bearings-further experiments, Proc. Inst. Mech. Eng. Conf. Proc. 178 (1963) 89–99, https://doi.org/10.1243/PIME_CONF_1963_178_380_02.
[7] J.K. Kim, S.J. Kim, The temperature dependence of the wear resistance of iron-base NOREM 02 hardfacing alloy, Wear 237 (2000) 217–222, https://doi.org/10.1016/S0043-1648(99)00326-9.
[8] L. Cachon, J. Denape, F. Sudreau, L. Lelait, Tribological qualification of cobalt-free coatings for pressurized water reactor primary-circuit gate valve applications, Surf. Coat. Technol. 85 (1996) 163–169, https://doi.org/10.1016/0257-8972(95)02672-X.
[9] K.Y. Lee, S.H. Lee, Y. Kim, H.S. Hong, Y.M. Oh, S.J. Kim, The effects of additive elements on the sliding wear behavior of Fe-base hardfacing alloys, Wear 255 (2003) 481–488, https://doi.org/10.1016/S0043-1648(03)00155-8.
[10] K.-Y. Lee, G. Guk Kim, J. Hui Kim, S.-H. Lee, S.-J. Kim, Sliding wear behavior of hardfacing alloys in a pressurized water environment, Wear 262 (2007) 845–849, https://doi.org/10.1016/j.wear.2006.08.015.
[11] C.B. Bahn, B.C. Han, J.S. Bum, I.S. Hwang, C.B. Lee, Wear performance and activity reduction effect of Co-free valves in PWR environment, Nucl. Eng. Des. 231 (2004) 51–65, https://doi.org/10.1016/j.nucengdes.2004.02.001.
[12] P. Crook, Cobalt and Cobalt Alloys, in: ASM Handb. Vol. 2 Prop. Sel. Nonferrous Alloy. Spec. Mater: 1990: pp. 446–454.
[13] R.T. Smith, T. Lolla, D. Gandy, L. Wu, G. Faria, A.J. Ramirez, S.S. Babu, P.M. Anderson, In situ X-ray diffraction analysis of strain-induced transformations in Fe- and Co-base hardfacing alloys, Scr. Mater. 98 (2015) 60–63, https://doi.org/10.1016/j.scriptamat.2014.11.003.
[14] K.J. Bhansali, A.E. Miller, The role of stacking fault energy on galling and wear behavior, Wear 75 (1982) 241–252, https://doi.org/10.1016/0043-1648(82)90151-X.
[15] D.H.E. Persson, On the Mechanisms behind the Tribological Performance of Stellites (Doctoral Thesis), Uppsala Universitet, 2005 (51 p).
[16] D.H.E. Persson, E. Coronel, S. Jacobson, S. Hogmark, Surface analysis of laser cladded Stellite exposed to self-mated high load dry sliding, Wear 261 (2006) 96–100, https://doi.org/10.1016/j.wear.2005.09.027.
[17] D.H.E. Persson, S. Jacobson, S. Hogmark, Antigalling and low friction properties of a laser processed Co-based material, J. Laser Appl. 15 (2003) 115–119, https://doi.org/10.2351/1.1514218.
[18] L. da Conceição, A.S.C.M. D'Oliveira, The effect of oxidation on the tribolayer and sliding wear of a Co-based coating, Surf. Coat. Technol. 288 (2016) 69–78, https://doi.org/10.1016/j.surfcoat.2016.01.013.
[19] Y. Birol, High temperature sliding wear behaviour of Inconel 617 and Stellite 6 alloys, Wear 269 (2010) 664–671, https://doi.org/10.1016/j.wear.2010.07.005.
[20] P. Crook, C.C. Li, The elevated temperature metal-to-metal wear behavior of selected hardfacing alloys, in: Wear Mater., American Society of Mechanical Engineers: 1983: pp. 272–279.
[21] F.H. Stott, C.W. Stevenson, G.C. Wood, Friction and wear properties of Stellite 31 at temperatures from 293 to 1073 K, Met. Technol. 4 (1977) 66–74.
[22] W.H. Hocking, F.W. Stanchell, E. McAlpine, D.H. Lister, Mechanisms of corrosion of Stellite-6 on lithiated high temperature water, Corros. Sci. 25 (1985) 531–557.
[23] C. Maffiotte, M. Navas, M.L. Castaño, A.M. Lancha, XPS characterization of oxide films formed in cobalt-based alloys during corrosion tests at high temperature, Surf. Interface Anal. 30 (2000) 161–166, https://doi.org/10.1002/1096-9918(200008)30:1<161::AID-SIA764>3.0.CO;2-O.
[24] N.S. McIntyre, D. Zetaruk, E.V. Murphy, X-Ray photoelectron spectroscopic study of the aqueous oxidation of Stellite-6 alloy, Surf. Interface Anal. 1 (1979) 105–110, https://doi.org/10.1149/1.2133027.
[25] N.K. Taylor, I. Armson, Corrosion product release from stellites and stainless steel in high pressure, high temperature lithiated water, in: Proceedings of the Water Chem. Nucl. React. Syst. 3 International Conference, British Nuclear Society, London: 1983: pp. 141–151.
[26] W.H. Hocking, D.H. Lister, Corrosion of Stellite-6 in lithiated and borated high--temperature water, Surf. Interface Anal. 11 (1988) 45–59, https://doi.org/10.1002/sia.740110106.
[27] D. Kaczorowski, J.P. Vernot, Wear problems in nuclear industry, Tribol. Int. 39 (2006) 1286–1293, https://doi.org/10.1016/j.triboint.2006.02.048.
[28] V.-E. Iordache, F. Wenger, P. Ponthiaux, A. Ambard, J. Peybernes, J. Vallory, Comparison between tribocorrosion mechanisms of Stellite 6 and Zircaloy 4 in LiOH-H_3BO_3 solutions, in: Passivation of Metals and Semiconductors, and Properties of Thin Oxide Layers - A Selection of Papers from the 9th International Symposium, Paris, France, 27 June – 1 July 2005; 2006, pp. 495–500.
[29] S. Xu, I.L. Kondratova, N. Arbeau, W. Cook, D.H. Lister, Corrosion of UNS R30006 in high-temperature water under intermittent mechanical contact, Corrosion 61 (2005) 444–451.
[30] E. Lemaire, M. Le Calvar, Evidence of tribocorrosion wear in pressurized water reactors, Wear 249 (2001) 338–344, https://doi.org/10.1016/S0043-1648(00)00544-5.
[31] S. Guadalupe Maldonado, S. Mischler, M. Cantoni, W.J. Chitty, C. Falcand, D. Hertz, Mechanical and chemical mechanisms in the tribocorrosion of a Stellite type alloy, Wear 308 (2013) 213–221, https://doi.org/10.1016/j.wear.2013.04.007.
[32] J. Schindelin, I. Arganda-Carreras, E. Frise, V. Kaynig, M. Longair, T. Pietzsch, S. Preibisch, C. Rueden, S. Saalfeld, B. Schmid, J.Y. Tinevez, D.J. White, V. Hartenstein, K. Eliceiri, P. Tomancak, A. Cardona, Fiji: an open-source platform for biological-image analysis, Nat. Methods 9 (2012) 676–682, https://doi.org/10.1038/nmeth.2019.
[33] R. Ahmed, H.L. De Villiers Lovelock, S. Davies, N.H. Faisal, Influence of Re-HIPing on the structure-property relationships of cobalt-based alloys, Tribol. Int. 57 (2013) 8–21, https://doi.org/10.1016/j.triboint.2012.06.025.
[34] M.A. Ashworth, J.C. Bryar, M.H. Jacobs, S. Davies, Microstructure and property relationships in hipped Stellite powders, Powder Metall. 42 (1999) 243–249,

https://doi.org/10.1179/003258999665585.
[35] D.A. Rigney, The roles of hardness in the sliding behavior of materials, Wear 175 (1994) 63–69.
[36] H. Ocken, Performance of NOREM™ Hardfacing Alloys TR-112993 Final Report, Electric Power Research Insitute, Palo Alto, USA, 1999.
[37] Velan Inc., EPRI NP-4993 Project 1935 Topical Report: Laboratory Evaluations of Cobalt-free, Nickel-based Hard-facing Alloys for Nuclear Applications, Electric Power Research Insitute, Palo Alto, USA, 1987.
[38] S. Kapoor, R. Liu, X.J. Wu, M.X. Yao, Temperature-dependence of hardness and wear resistance of Stellite alloys, World Acad. Sci. Eng. Technol. 67 (2012) 964–973.
[39] R. Liu, X.J. Wu, S. Kapoor, M.X. Yao, R. Collier, Effects of temperature on the hardness and wear resistance of high-tungsten Stellite alloys, Metall. Mater. Trans. A Phys. Metall. Mater. Sci. 46 (2014) 587–599, https://doi.org/10.1007/s11661-014-2664-8.
[40] T. Yonezawa, T. Iwamura, N. Kojima, S. Suzuki, Applicability of cobalt free wear resistant materials to valves, in: Contrib. Mater. Investig. to Resolut. Probl. Encount. Press. Water React, in: Proceedings of the International Symp. Pap., Societe Francaise d'Energie Nucleaire (SFEN), Fontevraud, France: 1994: pp. 116–123.
[41] U. Malayoglu, A. Neville, G. Beamson, Characterisation of the passive film on HIPed Stellite 6 alloy using X-ray photoelectron spectroscopy, Mater. Sci. Eng. A 393 (2005) 91–101, https://doi.org/10.1016/j.msea.2004.09.071.